2. Title page

Effect of Shot Peening using Ultra-fine Particles on Fatigue Properties of 5056 Aluminum Alloy under Rotating Bending

Shoichi KIKUCHI [a,*] Yuki NAKAMURA [b], Koichiro NAMBU [c] and Masafumi ANDO [d]

[a] Department of Mechanical Engineering, Graduate School of Engineering, Kobe University, 1-1 Rokkodai-cho, Nada-ku, Kobe-shi, Hyogo, 657-8501, JAPAN

E-mail address: kikuchi@mech.kobe-u.ac.jp

*: Corresponding author, Phone: +81-78-803-6329, Fax: +81-78-803-6155

[b] Department of Mechanical Engineering, National Institute of Technology, Toyota College, 2-1 Eisei-cho, Toyota-shi, Aichi, 471-8525 JAPAN

[c] Department of Mechanical Engineering, National Institute of Technology, Suzuka College, Shiroko-cho, Suzuka-shi, Mie, 510-0294, JAPAN

[d] Innovation Team, IKK SHOT Co. Ltd., 412-4, Nunowari, Minami-Shibata-machi, Tokai-shi, Aichi, 476-0001, JAPAN

Abstract

Shot peening using particles 10 μm in diameter (ultra-fine particle peening: Ultra-FPP) was introduced to improve the fatigue properties of 5056 aluminum alloy. The surface microstructures of the Ultra-FPP treated specimens were characterized using a micro-Vickers

hardness tester, scanning electron microscopy (SEM), X-ray diffraction (XRD), non-contact scanning white light interferometry, and electron backscatter diffraction (EBSD). The Ultra-FPP treated specimen had higher hardness than the conventional FPP treated specimen with a short nozzle distance due to the high velocity of the ultra-fine particles. Furthermore, the surface hardness of the Ultra-FPP treated specimen tended to increase as the peening time decreased. Fatigue tests were performed in air at room temperature using a cantilever-type rotating bending fatigue testing machine. It was found that the fatigue life of the Ultra-FPP treated specimen tended to increase with decreasing peening time. Mainly, the Ultra-FPP improved the fatigue properties of 5056 aluminum alloy in the very high cycle regime of more than 10^7 cycles compared with the un-peened specimens. This is because the release of the compressive residual stress is small during fatigue tests at low stress amplitudes.

Keywords

Shot peening, Fine particle peening, Fatigue, Aluminum alloy, Residual stress, Hardness

3. Text, double-spaced

1. Introduction

Recently, the reduction of greenhouse gas (GHG) production has become one of the most important subjects regarding efforts to combat global climate change. Since the use of light-metal alloys as structural parts of mechanical components is effective for weight saving, improving efficiency and decreasing GHG emissions, it would be beneficial to improve their fatigue strength because most machine and structural parts exhibit fatigue failure in the fields of engineering. Shot peening is one of the most common surface modification techniques for improving the fatigue properties of materials [1-14], due to the formation of a surface-hardened layer and the generation of compressive residual stress.

Fine particle peening (FPP) is more effective for improving the fatigue properties of materials than conventional shot peening [1]. FPP is very similar to the conventional shot peening method except that the shot particles used in FPP (less than 200 μm in diameter) are much smaller than those used in shot peening (e.g. 510 μm [15], 600 μm [3], 700 μm [10], 800 μm [1,16,17] and 4 mm [13] in diameter). In previous reports, the effects of the shot particle size on the microstructural changes and fatigue properties of materials were investigated [1, 15,16,18]. Yonekura et al. [1] reported that the fatigue strength of FPP treated ferrite-pearlite steel was higher than that of the same material treated with conventional shot peening due to the generation of higher and more stable compressive residual stress on the

treated surface. Moreover, FPP is very effective for creating fine crystal grains [15,16,18,19] because the particle velocity in FPP is higher than that in conventional shot peening [17,20,21].

Based on these reports, it is expected that the fatigue strength will be improved by performing shot peening using finer shot particles. In this study, ultra-fine particle peening (Ultra-FPP) using particles 10 μm in diameter was introduced to improve the fatigue properties of 5056 aluminum alloy. However, various peening conditions influence surface properties such as surface roughness, hardness and residual stress, which all affect fatigue properties [9-11]. Therefore, the effects of Ultra-FPP on the surface properties of the material should be examined to determine the condition that achieves the highest fatigue strength.

The purpose of this study is to examine the effects of Ultra-FPP on the surface microstructure of 5056 aluminum alloy. Furthermore, the fatigue properties of 5056 aluminum alloy treated with Ultra-FPP in the very high cycle regime (around 10^9 cycles or giga-cycles) were experimentally investigated by performing fatigue tests under rotating bending.

2. Experimental procedures

2.1 Material and specimen preparation

5056 aluminum alloy with the certificated chemical composition shown in Table 1 was used in this work. The certificated mechanical properties of this material are shown in Table 2. Figure 1 shows a cross-sectional optical micrograph of this alloy with a 78 μm

average grain size.

Table 1 Chemical composition of 5056 aluminum alloy (mass%).

Si	Fe	Cu	Mn	Mg	Cr	Zn	Al
0.04	0.13	0.01	0.06	4.8	0.06	0.02	Bal.

Table 2 Mechanical properties of 5056 aluminum alloy

Tensile strength (MPa)	0.2% proof stress (MPa)	Elongation (%)	Vickers hardness (HV)
310	218	21	88

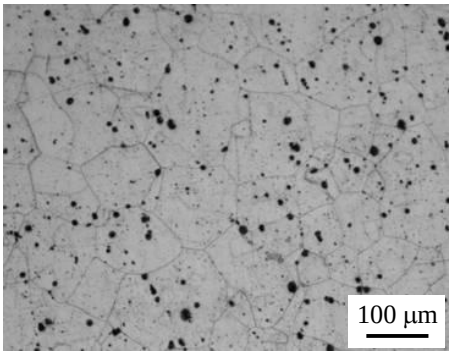

Fig.1 Cross-sectional optical micrograph of 5056 aluminum alloy.

Material rods 12 mm in diameter were machined into 5 mm thick disks for analyzing the surface microstructure and into hourglass-type specimens for fatigue tests and residual stress measurement. Figure 2 shows the configuration of the hourglass-type specimen. The diameter of the critical portion with a round notch at the center is 4.5 mm. After machining, these specimens were annealed at 473 K for 2 hours.

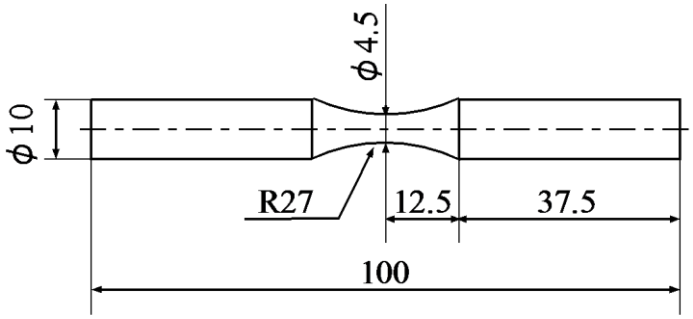

Fig.2 Specimen configuration for fatigue tests and residual stress measurement.

Ultra-FPP was performed for the disk and hourglass-type specimens under the conditions given in Table 3. In this study, we changed the particle diameter, nozzle distance, peening pressure, and peening times. Figure 3(a) shows a scanning electron microscopy (SEM) micrograph of the 10 μm diameter shot particles, which had a Vickers hardness of 862 HV and the chemical composition, which was measured by the of authors, shown in Table 4. For comparison, 50 μm diameter shot particles used for conventional FPP were also prepared, as shown in Figure 3(b).

Table 3 Peening conditions for (a) disk specimen and (b) hourglass-type specimen.

(a)

Series	Particle diameter, μm	Nozzle distance, mm	Peening pressure, MPa	Peening time, s
Ultra-FPP	10	30	0.6	3
				10
				30
		50	0.2	3
			0.4	
			0.6	
FPP	50	50	0.2	3
			0.4	
			0.6	

(b)

Series	Particle diameter, μm	Nozzle distance, mm	Peening pressure, MPa	Peening time, s
Ultra-FPP	10	30	0.6	5
				10
				30
		50	0.2	10
			0.4	
			0.6	
FPP	50	50	0.6	10

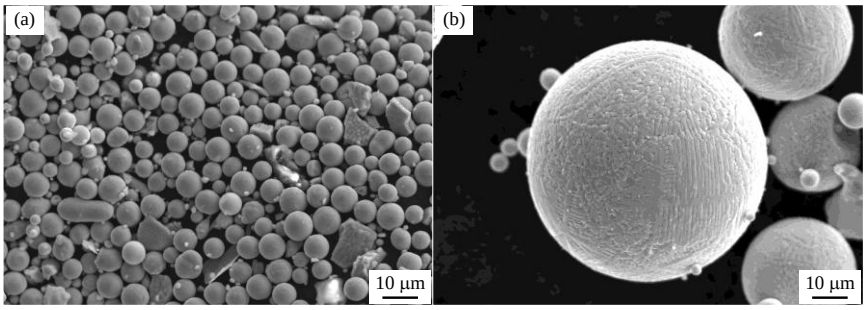

Fig.3 SEM micrographs of shot particles using (a) Ultra-FPP and (b) conventional FPP.

Table 4 Chemical composition of shot particles (mass%).

C	Si	Mn	P	S	Fe
0.99	1.19	0.54	0.016	0.011	Bal.

2.2 Characterization of the surface-modified layer

The hardness distributions were measured along the longitudinal section of the disk specimen using a micro-Vickers hardness tester at a load of 0.098 N. The surface microstructure of the specimens was characterized using SEM, non-contact scanning white light interferometry, and electron backscatter diffraction (EBSD). The residual stress was also measured for the transverse section of the smallest diameter of the hourglass-type specimen by X-ray diffraction (XRD) using CrKα radiation with a position-sensitive proportional counter (PSPC) system based on the $\sin^2\psi$ method [22,23]. The conditions for measuring the residual stress are shown in Table 5.

Table 5 Residual stress measurement conditions.

Tube voltage, kV	40
Tube current, mA	30
Diffraction angle 2θ, deg	156.6
Incident angle, deg	10, 20, 30, 35, 40
Beam diameter, mm	ϕ0.5
Stress constant, MPa / deg	-94.86

2.3 Fatigue tests

Fatigue tests were performed using a dual-spindle rotating bending fatigue testing

machine. This fatigue testing machine has two spindles driven by an electric motor via a V-belt, and each spindle has specimen grips at both ends. This machine can simultaneously perform fatigue tests on four specimens under rotating bending. The eccentricity of the specimens mounted to the specimen grips was kept within 20 μm at the tip of the specimen. This type of testing machine was originally developed to perform a series of long-term fatigue tests within a definite period [24].

Fully reversed fatigue tests under rotating bending were performed in air without any control of the temperature or moisture, at a stress ratio of R = -1, which is the ratio of minimum stress to maximum stress applied to the specimen surface. The rotation speed of the spindle under rotating bending was 52.5 Hz. After testing, the fracture surfaces of the failed specimens were observed by SEM.

3. Results and discussion

3.1 Effect of shot particle diameter on the surface microstructure of the shot-peened aluminum alloy

The effect of the shot particle size on the surface microstructure of the aluminum alloy was first examined. Figure 4 shows SEM micrographs of the surfaces treated with (a)-(c) Ultra-FPP and (d)-(f) conventional FPP for 3 s at various peening pressures with a 50 mm nozzle distance, and alongside (g) the un-peened specimen. The surface dents formed by Ultra-FPP (using particles 10 μm in diameter) were smaller than those induced by

conventional FPP (using particles 50 μm in diameter). Moreover, the size of the surface dents tended to increase with the peening pressure. Figure 5 shows the relationship between the arithmetic mean deviation *Ra* measured for the shot-peened surfaces and the peening pressure. In both series, the value of *Ra* tended to increase with peening pressure, and the *Ra* value for the Ultra-FPP treated specimen was lower than that for the conventional FPP treated specimens. It was found that the surface topography of the shot-peened specimens depended on the particle diameter and peening pressure.

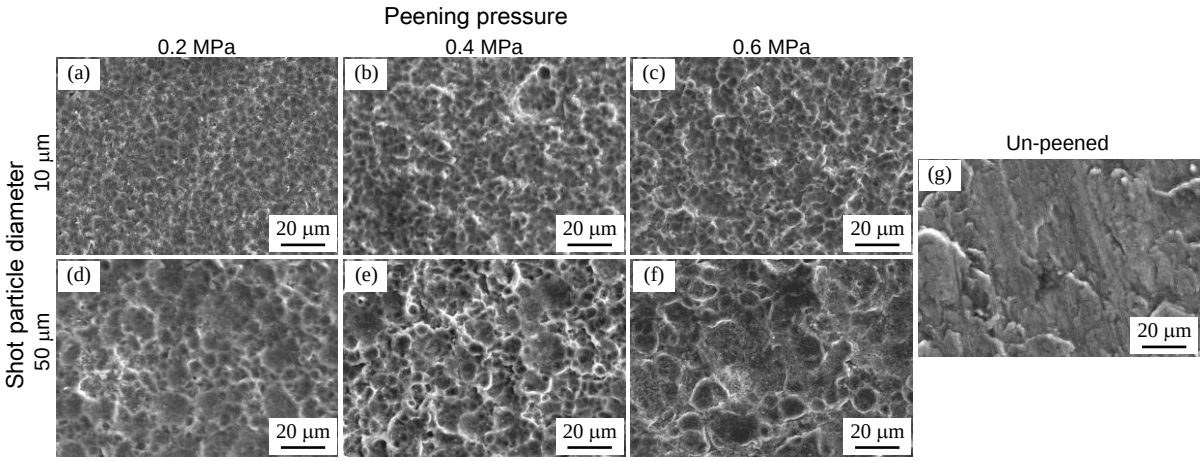

Fig.4 SEM micrographs of shot-peened surface (nozzle distance: 50 mm, peening time: 3 s).

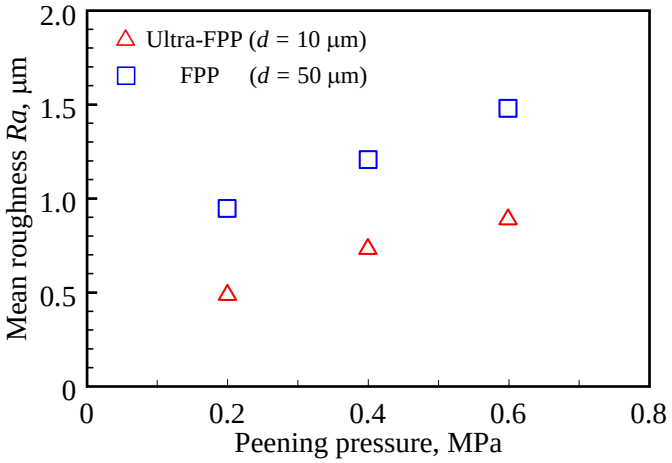

Fig.5 Relationship between arithmetic mean deviation *Ra* measured for shot-peened surfaces and peening pressure (nozzle distance: 50 mm, peening time: 3 s).

Figure 6 shows the Vickers hardness distribution for various longitudinal-sectional depths for disk specimens treated with Ultra-FPP and FPP for 3 s. The surface hardness increased with conventional FPP, and the thickness of the hardened layer was approximately 25 μm. In contrast, the Ultra-FPP treated specimen had almost the same hardness as the un-peened specimen (represented by a dotted line in this figure). Figure 7 shows the results for the measured residual stresses generated for the surfaces treated with Ultra-FPP for 10 s at various peening pressures. For comparison, the data for the specimen treated with FPP at 0.6 MPa and un-peened specimen are also indicated in Figure 7. It was found that compressive residual stress generated at the surface of each Ultra-FPP treated specimen was higher than that of the un-peened specimen represented by a dotted line in Figure 7, and tended to increase with peening pressure. However, in the case of the 0.6 MPa series, the compressive residual stress generated in the Ultra-FPP treated specimens was low compared with that for the conventional FPP treated specimens. Figures 6 and 7 indicate that Ultra-FPP does not remarkably modify the surface microstructure of 5056 aluminum alloy compared with conventional FPP at a 50 mm nozzle distance.

In order to clarify the reason for this, the velocity of the shot particles was analyzed based on the model that the authors' research group has proposed [20,21]. In our numerical calculation, the velocity of shot particles with various diameters through a convergent nozzle was analyzed from the following formula (1), in assuming that the air passing through the nozzle was considered as a compressible fluid.

$$dV/dx = 3C_D\rho_a(U-V)^2/4\rho_b Vd \qquad (1)$$

where V is particle velocity (m/s), U is air velocity (m/s), x is distance (m), C_D is drag coefficient, ρ_a is air density (kg/m^3), ρ_b is particle density (kg/m^3), and d is particle diameter (m).

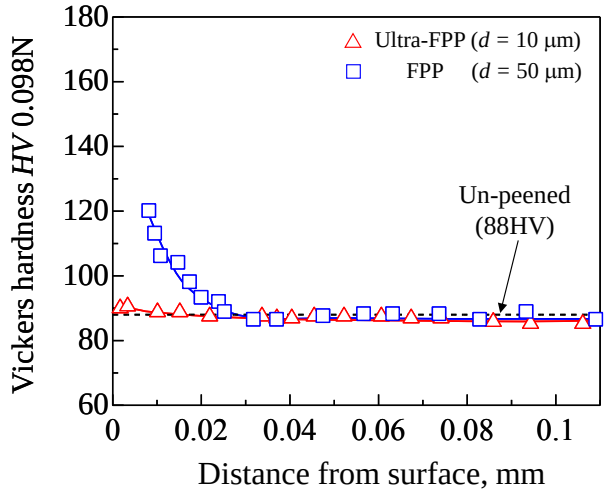

Fig.6 Distributions of Vickers hardness at various longitudinal-sectional depths (nozzle distance: 50 mm, peening pressure: 0.6 MPa, peening time: 3 s).

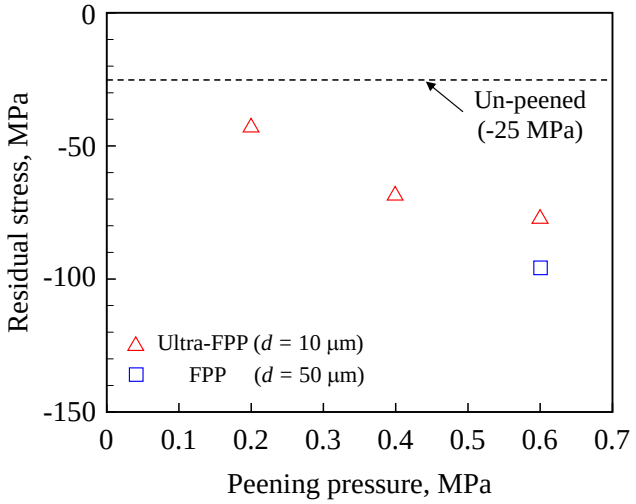

Fig.7 Residual stress measured for shot-peened surface (nozzle distance: 50 mm, peening time: 10 s).

Figure 8 shows the estimated velocity for shot particles of different diameters under 0.6 MPa compressed air. This figure shows that the velocity of the shot particles tended to increase as their diameter decreased. For particles larger than 50 μm in diameter, the velocity gradually increased as the distance from the nozzle tip increased and then kept a constant value. In contrast, the velocity of the ultra-fine particles (10 μm in diameter) tended to increase with increasing distance and tended to decrease as the velocity of the compressed air decreased. This result indicates that the velocity of the ultra-fine particles depends strongly on the compressed air pressure. Moreover, the velocity of the ultra-fine particle was highest at a distance of 30 mm from the tip of nozzle (130 mm on the horizontal axis in Fig. 8). This is why Ultra-FPP does not remarkably modify the surface microstructure of aluminum alloy at a 50 mm nozzle distance.

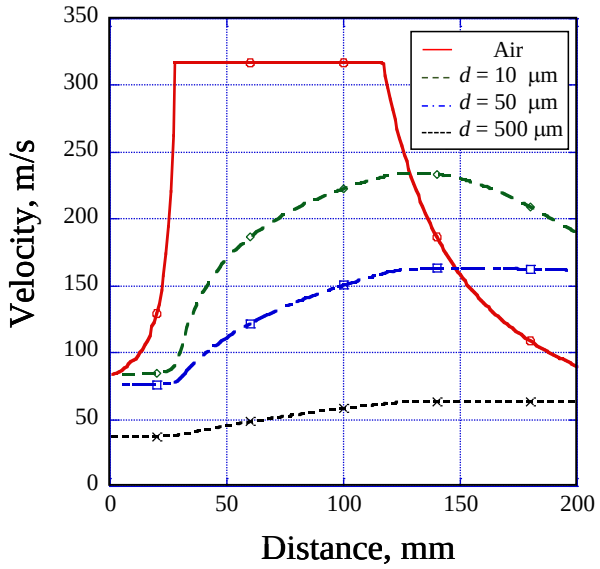

Fig.8 Estimated velocity of shot particles (peening pressure: 0.6 MPa).

3.2 Effect of nozzle distance and peening time on the surface microstructure of the shot-peened aluminum alloy

Based on the results obtained in the previous section, Ultra-FPP was performed with the highest velocity and at a shorter nozzle distance (30 mm) at a peening pressure of 0.6 MPa. Figure 9 shows the relationship between arithmetic mean deviation *Ra* measured at the top surfaces and the peening time for the Ultra-FPP treated specimens at a nozzle distance of 30 mm. For comparison, the data for the specimen treated with FPP for 3 s at a nozzle distance of 50 mm is also indicated in Figure 9 again. In the case of the 3 s series, the value of *Ra* for a nozzle distance of 30 mm was higher than that for the 50 mm series. This was because the particle velocity at a nozzle distance of 30 mm was higher than that at 50 mm at a peening pressure of 0.6 MPa, as shown in Figure 8. Moreover, it was found that the *Ra* value for the 30 mm series was almost the same regardless of the peening time. These results indicate that the amount of plastic deformation at the surface is saturated when performing Ultra-FPP at a nozzle distance of 30 mm.

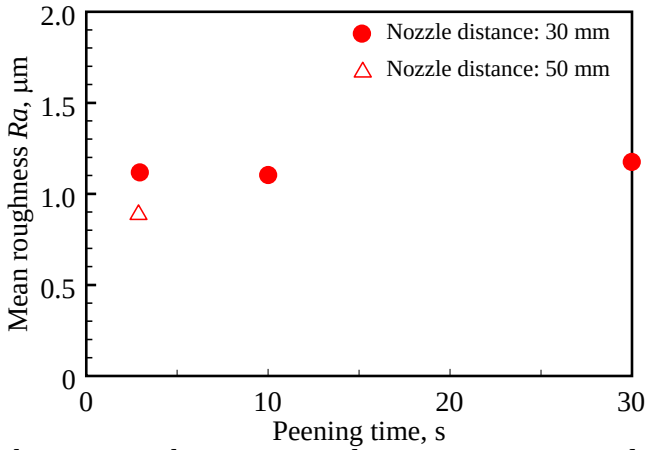

Fig.9 Relationship between arithmetic mean deviation *Ra* measured for Ultra-FPP treated surfaces and peening time (peening pressure: 0.6 MPa).

Figure 10 shows the distribution of Vickers hardness at various longitudinal-sectional depths for the Ultra-FPP treated disk specimens at a 30 mm nozzle distance. The Ultra-FPP increased the surface hardness of the specimens. The surface hardness and thickness of the hardened layer for the Ultra-FPP treated specimen tended to decrease as the peening time increased. This result indicates that Ultra-FPP is effective for increasing the surface hardness of 5056 aluminum alloys at a short nozzle distance and peening time.

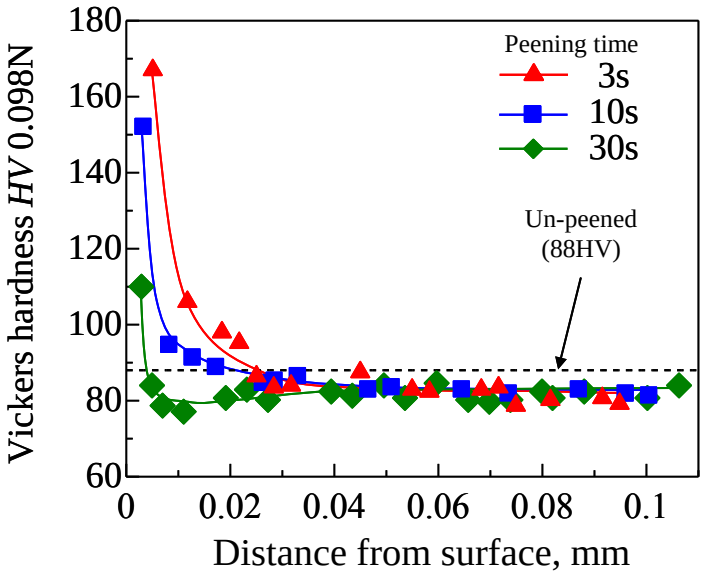

Fig.10 Distributions of Vickers hardness at various longitudinal-sectional depths (nozzle distance: 30 mm, peening pressure: 0.6 MPa).

Figure 11 shows inverse pole figure (IPF) maps obtained by EBSD for the longitudinal section of the specimen treated with Ultra-FPP for 3 s at (a) low and (b) high magnifications. In this figure, the dotted line indicates the outline of the specimen surface. The IPF map of the surface layer was not clearly obtained because Ultra-FPP induced high strain near the specimen surface. The thickness of this unclear region on the IPF map was

about 10 μm corresponding to a high hardness layer, as shown in Figure 10. Moreover, fine crystal grains were observed beneath this unclear region. Consequently, ultra-FPP can create fine crystal grains with high hardness within a relatively short time (3 s) at a short nozzle distance.

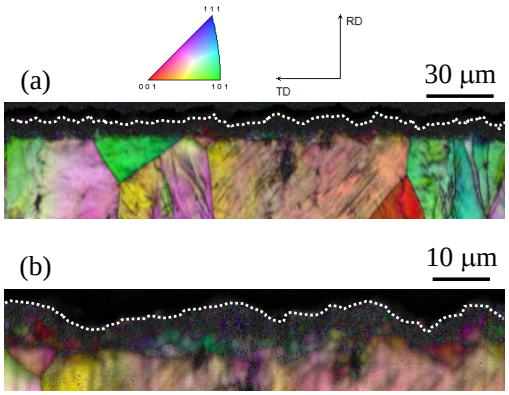

Fig.11 Inverse pole figure (IPF) maps obtained by EBSD for Ultra-FPP treated specimen at (a) low and (b) high magnifications for a longitudinal section (nozzle distance: 30 mm, peening pressure: 0.6 MPa, peening time: 3 s).

3.3 Effect of Ultra-FPP on the fatigue properties of aluminum alloy under rotating bending

In order to investigate the effect of Ultra-FPP on the fatigue properties of 5056 aluminum alloy, rotating bending fatigue tests were performed on the specimens treated with Ultra-FPP at a 30 mm nozzle distance. The results of the fatigue tests under rotating bending are plotted as *S*-*N* diagrams for the (a) un-peened and (b) Ultra-FPP treated specimens in Figure 12. In (a), the plot with the arrow represents a run-out specimen without failure. Moreover, at a stress amplitude of 220 MPa, fatigue tests were conducted for 13 un-peened specimens to evaluate the scatter of the fatigue life. In the case of the un-peened specimens,

the fatigue limit was not clearly observed because the *S-N* curve tended to decrease continuously toward the giga-cycle regime. Based on such experimental evidence, the *S-N* curve was determined by accepting the *S-N* model without a fatigue limit in the JSMS standard regression models [25]. The regression *S-N* curve for the un-peened specimen is expressed by the following formula:

$$\text{Un-peened series: } \log(\sigma_a - 119.77) = -0.18092\log(N) + 2.8697 \qquad (2)$$

where σ_a is the stress amplitude (MPa), and N is the number of cycles. The strength at 10^7 cycles of the un-peened specimen is 160 MPa estimated by equation (2).

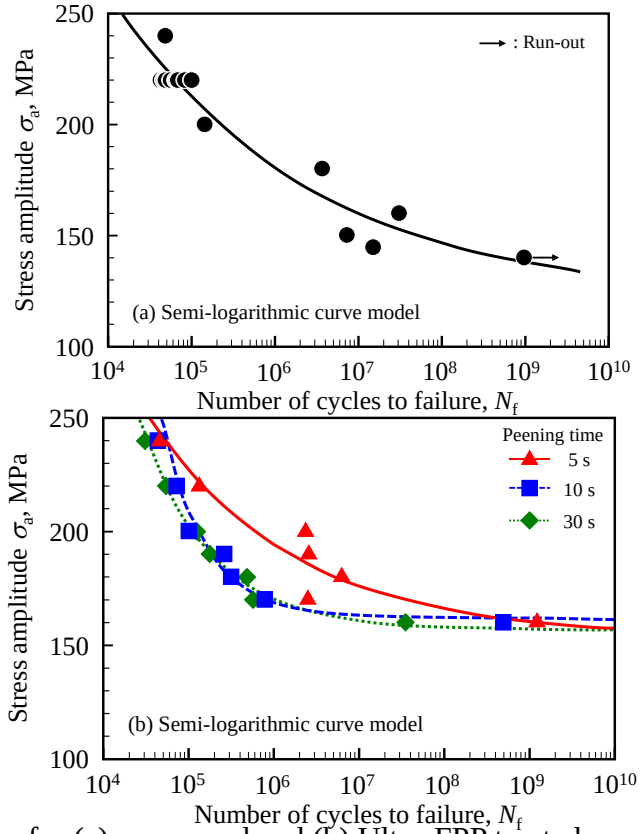

Fig.12 *S-N* diagram for (a) un-peened and (b) Ultra-FPP treated specimens (nozzle distance: 30 mm, peening pressure: 0.6 MPa).

In contrast, the fatigue lives of the Ultra-FPP treated specimens were divided into two groups: failure in the short life regime and failure in the long life regime, as shown in Figure 12(b); however, since every specimen failed in the surface fracture mode as mentioned in Figure 14. Based on this tendency, the *S-N* curve was determined by accepting a curve model without the fatigue limit based on the JSMS standards [25] as well as the un-peened specimen. The regression *S-N* curves for the Ultra-FPP treated specimens are expressed by the following formula (3)-(5):

$$\text{5 s series: } \log(\sigma_a - 153.46) = -0.25247\log(N) + 3.1321 \quad (3)$$

$$\text{10 s series: } \log(\sigma_a - 162.07) = -0.84408\log(N) + 5.8924 \quad (4)$$

$$\text{30 s series: } \log(\sigma_a - 156.88) = -0.52708\log(N) + 4.2993 \quad (5)$$

where σ_a is the stress amplitude (MPa), and N is the number of cycles. The strengths at 10^7 cycles of the Ultra-FPP treated specimens for 5, 10 and 30 s are 177, 163 and 161 MPa, respectively.

Every Ultra-FPP treated specimen showed higher strength at 10^7 cycles than that for the un-peened specimen (160 MPa). The fatigue life for the Ultra-FPP treated specimen at a stress amplitude of 160 MPa tended to increase as the peening time decreased. Especially, the 5 s series failed in the very high cycle regime of more than 10^9 cycles. However, another finding in Figure 12 showed that the Ultra-FPP treated specimens showed almost the same

fatigue life as the un-peened specimen in the short life regime, whereas Ultra-FPP significantly improved the fatigue properties of 5056 aluminum alloy in the very high cycle regime. In order to quantify the effect of Ultra-FPP on the fatigue properties of A5056 aluminum alloy, the improvement in strength at given cycles by Ultra-FPP was calculated. Figure 13 shows the relationship between the improvements in fatigue strength by Ultra-FPP and number of cycles. In the case of the 5 s series, the improvement in strength by Ultra-FPP was positive at the whole number of cycles and increased gradually with number of cycles. On the other hand, strength was not improved by Ultra-FPP in the 10 and 30 s series in the short life regime, whereas the improvement was positive in the high cycle regime more than 10^7 cycles and tended to increase with increasing number of cycles, resulting in improving approximately 20% fatigue strength of 5056 aluminum alloy in the very high cycle regime. It can be concluded that Ultra-FPP is effective at improving the very high cycle fatigue properties of 5056 aluminum alloy using a short nozzle distance and peening time.

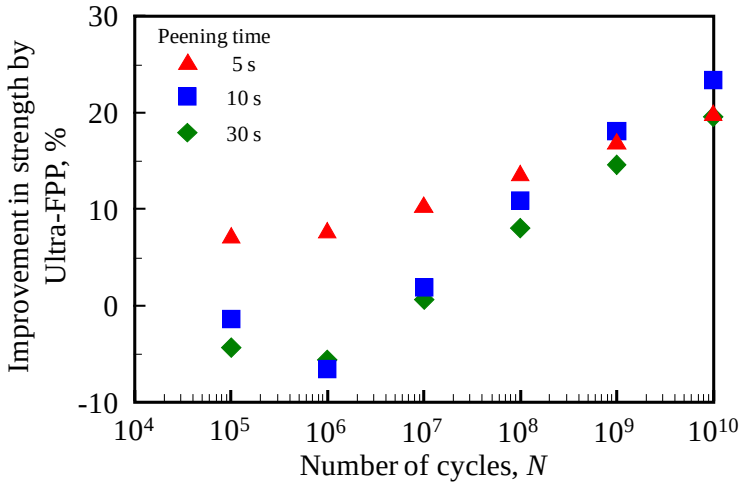

Figure 13 Relationship between improvement in strength by Ultra-FPP and number of cycles.

Figure 14 shows typical features of the fatigue crack initiation site for the (a) un-peened and (b) Ultra-FPP treated specimens. In this study, every specimen failed in surface fracture mode. In the very high cycle regime, high-strength steels often exhibit duplex *S-N* properties consisting of surface-initiated and interior-initiated fracture modes [26]. However, 5056 aluminum alloys have failed in the surface-initiated fracture mode even in the very high cycle regime, as shown in Figure 14(b). Thus, such duplex *S-N* curves were not clearly found for this alloy.

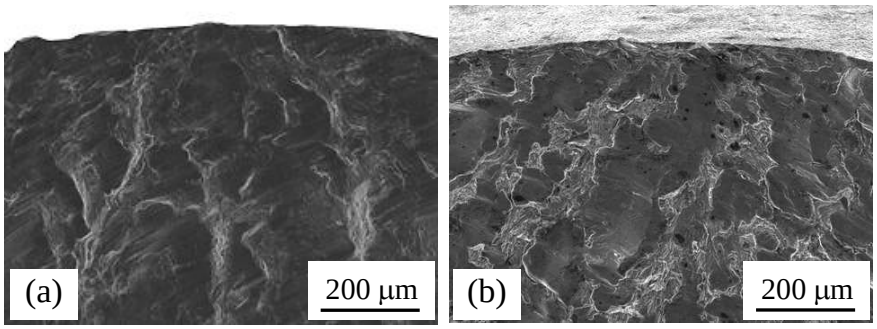

Fig.14 Typical features of fracture surfaces for (a) un-peened specimen failed at N_f = 3.1x10^7 and (b) Ultra-FPP treated specimen failed at N_f = 1.2x10^9 (stress amplitude: 160 MPa, nozzle distance: 30 mm, peening pressure: 0.6 MPa, peening time: 5 s).

3.4 Relaxation of compressive residual stress generated by Ultra-FPP

It is well known that compressive residual stress generated by shot peening is released during fatigue tests [1,9-14]. In order to examine the relaxation of compressive residual stresses during fatigue tests, the compressive residual stress was measured at the same position in the Ultra-FPP treated specimens at N = 0 and 10^4 cycles under stress

amplitudes of 160 and 220 MPa.

Figure 15 shows the relationship between the compressive residual stress and the stress amplitude. In this figure, the data for a stress amplitude of 0 MPa indicates the initial compressive residual stress. First, the compressive residual stress tended to increase with peening time before fatigue tests. The compressive residual stress after the fatigue tests was lower than that before the fatigue tests. This result indicates that the compressive residual stress is released in the early stage of the fatigue tests. In addition, it was found that the compressive residual stress is more significantly released at a high stress amplitude (220 MPa) than at a low stress amplitude (160 MPa). This is why Ultra-FPP does not improve the fatigue life of 5056 aluminum alloy in the short life regime for a high stress amplitude.

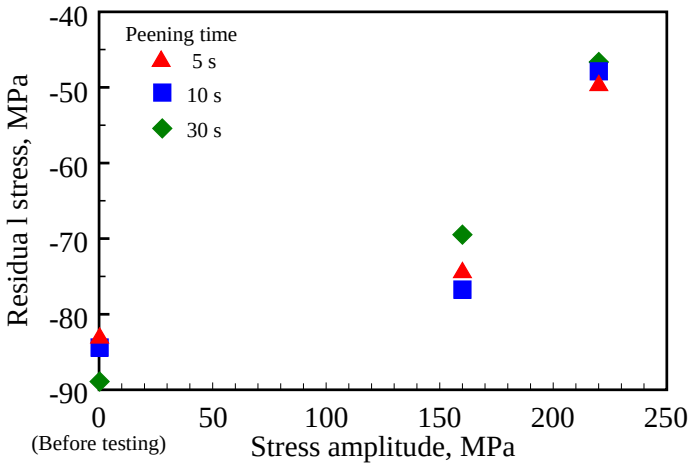

Fig.15 Relationship between compressive residual stress and stress amplitude after fatigue tests at $N = 10^4$ cycles (nozzle distance: 30 mm, peening pressure: 0.6 MPa).

Figure 16 shows the relationship between the reduction in compressive residual

stress and the peening time. It was found that the amount of released compressive residual stress tended to increase with peening time. This may be because yielding occurs in compression during fatigue tests (R = -1). Generally, when the sum of the compressive residual stress and the applied stress in compression during fatigue tests exceeds the yield stress, the residual stress is released. Since the static strength is proportional to the Vickers hardness, the local surface strength of the Ultra-FPP treated specimen is thought to increase as the peening time decreases based on the hardness distribution, as shown in Figure 10. Then, the compressive residual stress generated in the 5 s series is more stable against cyclic loading.

Consequently, the compressive residual stress generated by Ultra-FPP was not significantly released at a low stress amplitude. This resulted in improved very high cycle fatigue properties of 5056 aluminum alloy by Ultra-FPP for a short nozzle distance and peening time.

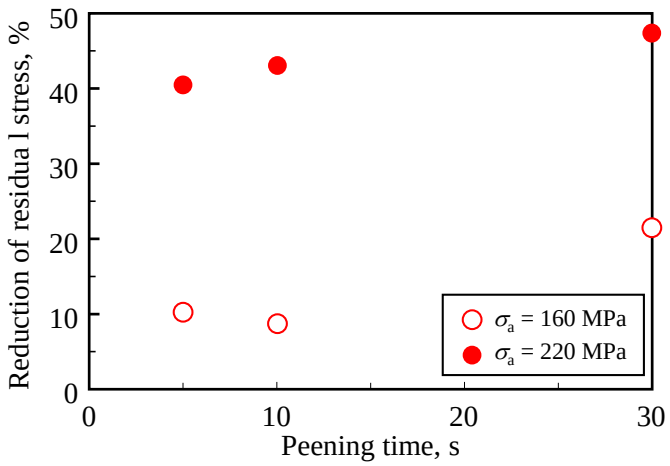

Fig.16 Relationship between reduction in compressive residual stress and stress amplitude at $N = 10^4$ cycles (nozzle distance: 30 mm, peening pressure: 0.6 MPa).

4. Conclusions

In this study, the effect of Ultra-FPP (shot peening using particles 10 μm in diameter) on the surface microstructure of 5056 aluminum alloy was investigated. Moreover, rotating bending fatigue tests were performed to examine the effect of Ultra-FPP on the fatigue properties of 5056 aluminum alloy. The main conclusions obtained in this study are summarized as follows:

1. Ultra-FPP is effective at increasing the surface hardness of 5056 aluminum alloy when using a short nozzle distance and peening time.

2. The fatigue life of the specimen treated with Ultra-FPP tends to increase as the peening time decreases.

3. Ultra-FPP improves approximately the 20% fatigue strength of 5056 aluminum alloy in the giga-cycle regime. This is because the release of the compressive residual stress is small for fatigue tests at a low stress amplitude for the specimen treated with Ultra-FPP using a short nozzle distance and peening time.

Acknowledgement

This research was supported by the Adaptable and Seamless Technology Transfer Program (A-STEP, No. AS232Z02366C) through Target-driven R&D, JST and the Japan Aluminum Association. The authors would like to thank JST and the Japan Aluminum Association for their support.

List of references

[1] D. Yonekura, J. Noda, J. Komotori, M. Shimizu, H. Shimizu, Trans. Jpn Soc. Mech. Eng. A 67 (2001) 1155-1161.

[2] Y. K. Gao, Mater. Sci. Eng. A 528 (2011) 3823-3828.

[3] K. Masaki, Y. Ochi, T. Matsumura, Fatigue Fract. Eng. Mater. Struct. 27 (2004) 1137-1145.

[4] P. Peyre, R. Fabbro, P. Merrien, H. P. Lieurade, Mater. Sci. Eng. A 210 (1996) 102-113.

[5] R. K. Nalla, I. Altenberger, U. Noster, G. Y. Liu, B. Scholtes, R. O. Ritchie, Mater. Sci. Eng. A 355 (2003) 216-230.

[6] J. M. Yang, Y. C. Her, Nanlin Han, A. Caluer, Mater. Sci. Eng. A 298 (2001) 296-299.

[7] S. Kikuchi, Y. Nakahara, J. Komotori, Int. J. Fatigue 32 (2010) 403-410.

[8] M. Benedetti, T. Bortolamedi, V. Fontanari, F. Frendo, Int. J. Fatigue 26 (2004) 889-897.

[9] H. Itoga, K. Tokaji, M. Nakajima, H. N. Ko, Int. J. Fatigue 25 (2003) 379-385.

[10] M. A. S. Torres, H J. C. Voorwald, Int. J. Fatigue 24 (2002) 877-886.

[11] S. Kikuchi, Y. Hirota, J. Komotori, J. Soc. Mater. Sci. Jpn, 60 (2011) 547-553.

[12] U. Martin, I. Altenberger, B. Scholtes, K. Kremmer, H. Oettel, Mater. Sci. Eng. A 246 (1998) 69-80.

[13] J. Arakawa, M. Kakuta, Y. Hayashi, R. Tanegashima, H. Akebono, M. Kato, A. Sugeta, Surf. Eng. 30 (2014) 662-669.

[14] J. C. Kim, S. K. Cheong, H. Noguchi, Int. J. Fatigue 56 (2013) 114-122.

[15] T. Morita, S. Noda, C. Kagaya, Mater. Trans. 55 (2014) 646-652.

[16] S. Kikuchi, Y. Hirota, J. Komotori, J. Jpn Soc. Abrasive Technol. 54 (2010) 720-724.

[17] T. Ito, S. Kikuchi, Y. Hirota, A. Sasago, J. Komotori, Int. J. Modern Physics B 24 (2010) 3047-3052.

[18] J. L. Liu, M. Umemoto, Y. Todaka, K. Tsuchiya, J. Mater. Sci. 42 (2007) 7716-7720.

[19] S. Kikuchi, J. Komotori, Mater. Trans. 56 (2015) 556-562.

[20] H. Maeda, N. Egami, C. Kagaya, N. Inoue, H. Takeshita, K. Ito, Trans. Jpn Soc. Mech. Eng. C 67 (2001) 2700-2706.

[21] K. Nambu, K. Ito, N. Egami, Trans. Jpn Soc. Mech. Eng. C 76 (2010) 3728-3735.

[22] S. M. Wong, Thin Solid Films 53 (1978) 65-71.

[23] Q. Luo and A. H. Jones, Surf. Coat. Technol. 205 (2010) 1403-1408.

[24] T. Yamamoto, A. Kokubu, T. Sakai, Y. Nakamura, Proc. VHCF-6 (2014) AAI06.

[25] JSMS Committees on Fatigue of Materials and Reliability Engineering: Standard Evaluation Method of Fatigue Reliability for Metallic Materials -Standard Regression Method of *S-N* Curves-, The Society of Materials Science, Japan (2008).

[26] T. Sakai, J. Solid Mech. Eng. Mater. 3 (2009) 1573-1587.

5. List of table and figure captions

distance: 30 mm, peening pressure: 0.6 MPa).

Fig.11 Inverse pole figure (IPF) maps obtained by EBSD for Ultra-FPP treated specimen at (a) low and (b) high magnifications for a longitudinal section (nozzle distance: 30 mm, peening pressure: 0.6 MPa, peening time: 3 s).

Fig.12 *S*-*N* diagram for (a) un-peened and (b) Ultra-FPP treated specimens (nozzle distance: 30 mm, peening pressure: 0.6 MPa).

Fig.13 Relationship between improvement in strength by Ultra-FPP and number of cycles.

Fig.14 Typical features of fracture surfaces for (a) un-peened specimen failed at $N_f = 3.1 \times 10^7$ and (b) Ultra-FPP treated specimen failed at $N_f = 1.2 \times 10^9$ (stress amplitude: 160 MPa, nozzle distance: 30 mm, peening pressure: 0.6 MPa, peening time: 5 s).

Fig.15 Relationship between compressive residual stress and stress amplitude after fatigue tests at $N = 10^4$ cycles (nozzle distance: 30 mm, peening pressure: 0.6 MPa).

Fig.16 Relationship between reduction in compressive residual stress and stress amplitude at $N = 10^4$ cycles (nozzle distance: 30 mm, peening pressure: 0.6 MPa).